Journal of Catalysis 426 (2023) 301–307

Contents lists available at ScienceDirect

Journal of Catalysis

journal homepage: www.elsevier.com/locate/jcat

Research article

Definitive adsorption states of intermediates on Ru nanocatalysts for progress of ammonia synthesis discovered by modulation excitation spectroscopy under reaction conditions

Tomohiro Goroh Noguchi [a], David S. Rivera Rocabado [b], Yuki Kojo [c], Atsushi Oyabe [c], Takayoshi Ishimoto [b], Miho Yamauchi [a,d,e,f,*]

[a] Institute for Materials Chemistry and Engineering (IMCE), Kyushu University, Motooka 744, Nishi-ku, Fukuoka 819-0395, Japan
[b] Graduate School of Advanced Science and Engineering, Hiroshima University, 1-4-1 Kagamiyama, Higashi-Hiroshima, Hiroshima 739-8527, Japan
[c] Department of Chemistry, Graduate School of Science, Kyushu University, Motooka 744, Nishi-ku, Fukuoka 819-0395, Japan
[d] Advanced Institute for Materials Research (WPI-AIMR), Tohoku University 2-1-1 Katahira, Aoba-ku, Sendai 980-8577, Japan
[e] Research Center for Negative Emissions Technologies (K-NETs), Kyushu University, Motooka 744, Nishi-ku, Fukuoka 819-0395, Japan
[f] International Institute for Carbon-Neutral Energy Research (WPI-I^{2}CNER), Kyushu University, Motooka 744, Nishi-ku, Fukuoka 819-0395, Japan

ARTICLE INFO

Keywords:
Ammonia synthesis
In situ IR
Modulation excitation spectroscopy
Ru catalysts
Associative dissociation mechanism

ABSTRACT

Diffuse reflectance infrared Fourier transform spectroscopy combined with modulation excitation spectroscopy realized observation of NH_3 production process on a Ru nanoparticle supported on MgO under operation conditions in the presence of both H_2 and N_2 (~400 °C, 0.1 MPa). Our study clearly indicated that N_2 dissociation is developed via transition from vertically adsorbed states of N_2 (**N_2-Ver**) on an on-top Ru site to horizontally adsorbed states via **N_2-Ver** on a bridge site, which is a critical step for the progress of AS reactions on Ru catalysts at low temperatures and persists in the presence of both N_2 and H_2.

1. Introduction

Ammonia is a versatile basic raw material for the production of fertilizers and pharmaceuticals,[1] and is also expected to be a next-generation carbon-free hydrogen carrier, which is an essential component for efficient long-distance transport of green and blue hydrogen.[2] Thus, reduction of energy consumption through the application of renewable energy to NH_3 production would further enhance the advantage of NH_3 utilization. In this context, ammonia synthesis (AS) catalysts workable under milder conditions are highly demanded. Aika reported that Ru-based catalysts can efficiently promote ammonia synthesis at lower temperatures and lower pressures (350 °C, 0.1 MPa)[3] compared to those on industrially used Harbor-Bosch catalysts (450 °C, 30 MPa).[4] The high efficiency of Ru catalysts was explained by appropriate bond energy between Ru and N atoms, which is neither too high nor too low for the promotion of NH_3 synthesis, and then can exhibit high reaction rates due to smooth adsorption of N_2 and desorption of NH_3 on the surface.[5] To improve the catalytic activity of Ru-based catalysts, metal oxide,[6] electrides,[7] alkali metals,[8] alkali earth metals,[9] lanthanoid oxide,[10] hydride,[11] oxyhydride[12] and nanoalloys[13] have been applied, which promotes activity or prevents hydrogen poisoning.[14] For further catalytic enhancement, a more specific understanding of reaction progress on the catalyst surface is probably essential.

The adsorption behavior of reactant molecules on AS catalysts has been studied by mass spectrometry employing isotope labelling for post-reaction gases,[15] infrared spectroscopy (IR) and so on.[16] Despite these intense efforts, identifying active species and active sites are still challenging because of their low concentrations and variable natures of the catalytic surface, where multiple catalytic steps are simultaneously developed under reaction conditions. Here, in this study, we demonstrate the time-resolved in-situ IR measurement under reaction conditions (400 °C, 0.1 MPa) to precisely understand the adsorption states of intermediates on Ru AS catalysts, which can be a basic data for the characterization of various types of AS catalysts.

Previously, we observed adsorbed states of N_2 or H_2 on the Ru AS catalyst using diffuse reflectance infrared Fourier transform spectroscopy (DRIFTS) combined with modulation excitation spectroscopy (MES) under nearly reaction conditions (250 °C, 0.1 MPa).[17] MES realizes highly sensitive observation using phase sensitive detection of

* Corresponding author at: Institute for Materials Chemistry and Engineering (IMCE), Kyushu University, Motooka 744, Nishi-ku, Fukuoka 819-0395, Japan.
E-mail address: yamauchi@ms.ifoc.kyushu-u.ac.jp (M. Yamauchi).

https://doi.org/10.1016/j.jcat.2023.07.020
Received 17 April 2023; Received in revised form 10 July 2023; Accepted 24 July 2023
Available online 25 July 2023

signals responding only to a periodic excitation generated by repeatedly introducing a reaction gas such as N_2 or H_2 and non-reactive reference gas such as Ar, which cancels off-resonant noise signals.[18] Furthermore, dynamics of the adsorbed species on the surface can be extracted by analyzing delays in phase of signals from absorbed intermediates compared to that from reference gas.[19] We currently constructed a DRIFTS system that is usable at high temperatures (less than 600 °C) in the presence of reactant gases. We then performed time-resolved DRIFTS by introducing 0.1 MPa reaction gas at 400 °C, namely, a reaction condition. Furthermore, co-adsorption behaviors of N_2 and H_2 on the catalyst surface were examined.

2. Results and discussion

2.1. Structural and catalytic properties of Ru/MgO

MgO-supported Ru nanoparticle (NP) catalysts (Ru/MgO) were prepared accordingly to a previous report (see SI for details).[13] The morphology of Ru NPs on Ru/MgO was observed by transmission electron microscopy (TEM), which confirmed uniform dispersion of Ru NPs on MgO (Fig. 1a and S1). The average particle size of Ru NPs was approximately 5.5 nm (Figure S2). Powder X-ray diffraction (XRD) patterns of Ru/MgO were well reproduced by overlapping weak diffractions originating from a hexagonal close-packed phase of Ru NPs and strong diffractions from a face-centered cubic phase of MgO, suggesting the formation of Ru NPs in the presence of MgO (Figure S3). Scanning electron microscopy together with energy dispersive X-ray spectroscopy revealed that the loading amount of Ru on the catalyst is 4.3 wt%. Catalytic performance on Ru/MgO was evaluated using a gas-flow reactor at 300–500 °C under the mixed gas flow condition (0.1 and 1.0 MPa, N_2:H_2 = 1:3). Ru/MgO exhibited the highest activity at 400 °C and decreased above 400 °C at 0.1 MPa whereas the highest performance at 1 MPa was observed at 450 °C (Fig. 1b). The higher catalytic activity on Ru/MgO at higher total pressures accords to reported results.[13,20] and the reaction order of Ru/MgO for N_2[21] was found to be analogous to the that obtained in previous studies, whereas the value for H_2 was slightly positive compared to our previous result (Figure S4).[13] The difference is possibly explained by considering difference in the loading amount of Ru; 4.3 wt% in this work but 2 wt% in the previous work. This is because a larger number of active sites formed on 4.3 wt%-Ru/MgO somewhat hinders the poisoning compared to that on 2 wt %-Ru/MgO. Activation energies estimated from Arrhenius plots at 0.1 and 1.0 MPa (Figure S5, Table S1) were in the range for those reported on Ru-based catalysts.[6] These results suggested Ru/MgO exhibits normal AS activities.

2.2. Adsorption of pure N_2 or H_2

DRIFTS-MES measurements were performed using a Fourier transform IR instrument equipped with gas switching valves (Fig. 1c). Approximately 25 mg of the sample was placed in a porous sample cup and enclosed in the DRIFTS cell. Prior to the measurement, the sample was pretreated under 10 vol% H_2-Ar gas flow at 600 °C. We kept flowing of both reaction and reference gases at a flow rate of 80 ccm during the measurements, whereas the mixing ratio of reaction and reference gases was optimized at each temperature. The details of the gas mixing ratios are summarized in Table S2. We measured 30 IR spectra for 78 s (or 135 s) with the flow of reaction gas and analogously with reference gas, where the spectra measured at the end in the reference gas period was used as a background, namely 60 spectra were obtained in one series and

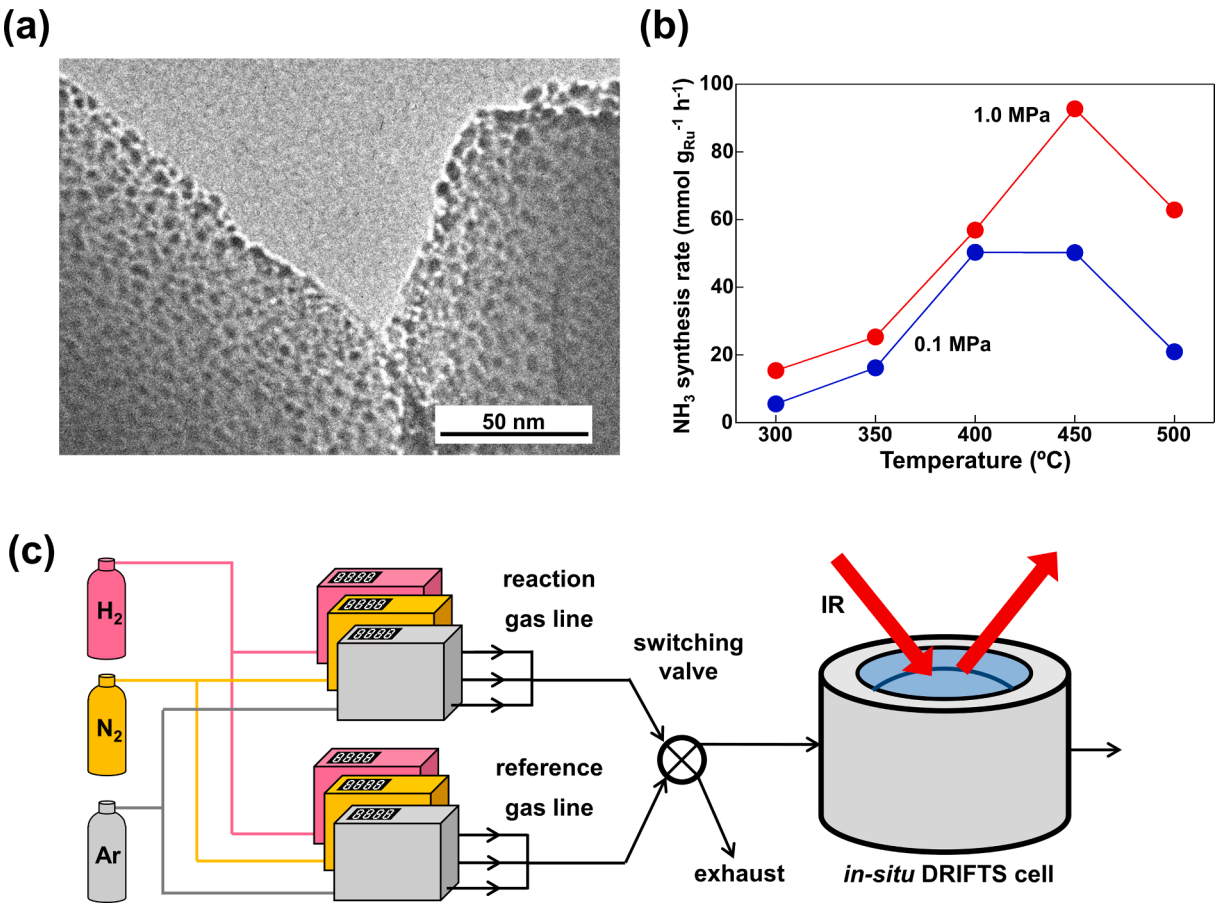

Fig. 1. Sample and measurement setup. (a) TEM image of Ru/MgO. (b) Temperature dependence in catalytic activity for NH_3 synthesis of Ru/MgO. (c) Schematic of the gas-switching type DRIFTS-MES system.

obtained data for 10 series. We produced a spectrum by accumulating signals obtained in the last 8 series.

Fig. 2a shows IR spectra for H_2 adsorption on Ru/MgO after Ar pre-adsorption at 400 °C together with the spectrum previously observed at 250 °C for comparison. Two peaks appeared around 2000 and 1850 cm^{-1} at both temperatures (Fig. 2a), which were assigned to adsorptions of H_2 molecules and dissociated H atoms (**H-Ru**), respectively, based on the result of density functional theory (DFT) calculations.[17] The peak at 1628 cm^{-1} observed at 250 °C was attributed to the bending vibration of OH species on MgO.[17] All signals decreased with time after switching to Ar flow, suggesting that desorption of adsorbed species occurred. It should be emphasized that adsorption and dissociation behaviors of H_2 at 250 and 400 °C looked similar, although no strong signal for the bending vibration of OH species was observed at 400 °C. In the spectra obtained in the presence of N_2, two obvious peaks appeared around 2071 and 1928 cm^{-1} at 250 °C (Fig. 2b), which were already

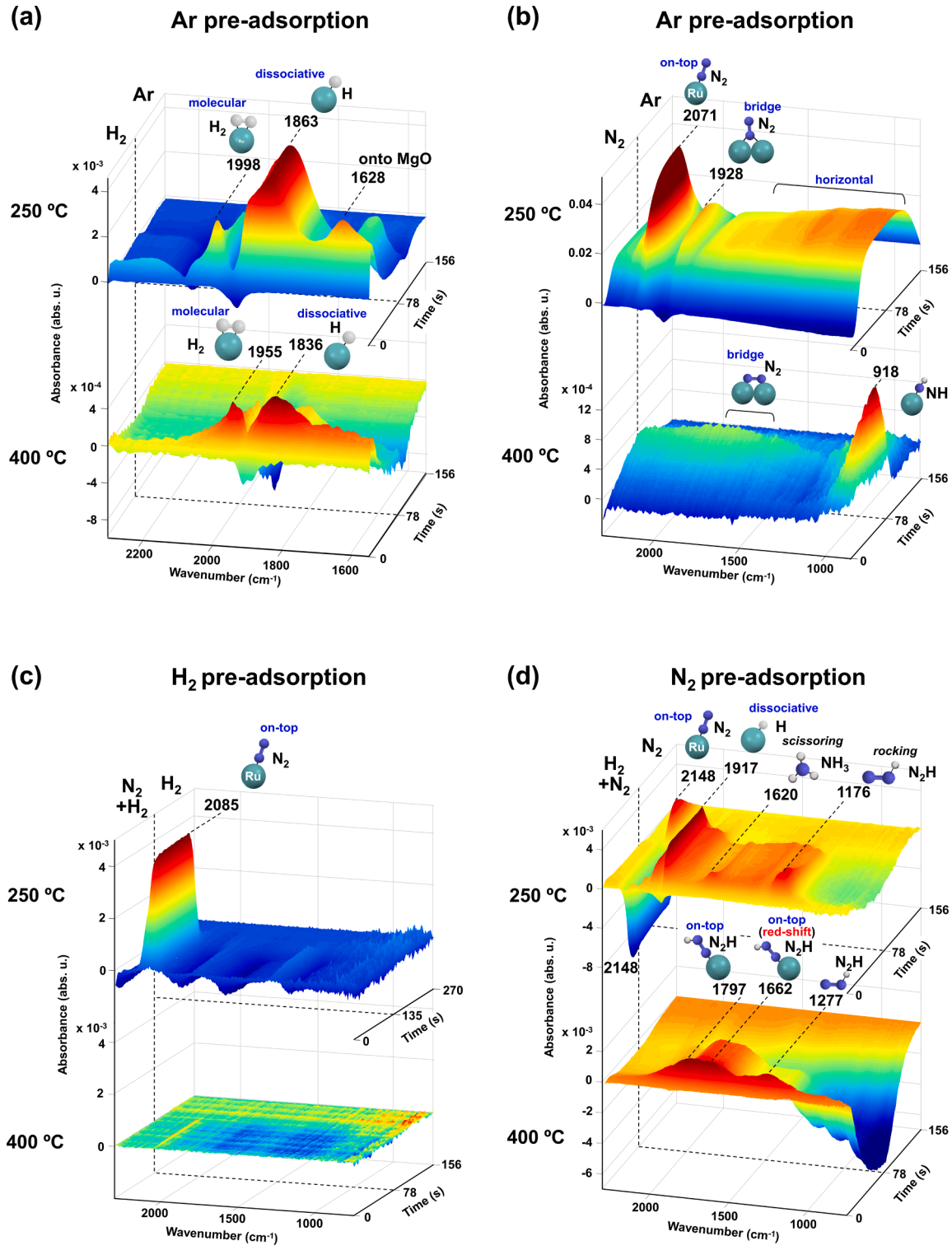

Fig. 2. Time-domain spectra on Ru/MgO surface at 250 and 400 °C under 0.1 MPa for (a) H_2 adsorption after Ar pre-adsorption, (b) N_2 adsorption after Ar pre-adsorption, (c) co-adsorption after H_2 pre-adsorption, and (d) co-adsorption after N_2 pre-adsorption.

attributed to vibrations of vertical adsorbed N_2 (**N_2-Ver**) on an on-top and bridge site of Ru NPs, respectively.[17] In addition, weak absorptions below 1500 cm^{-1} at 250 °C were assigned to vibrational states of horizontally adsorbed N_2 (**N_2-Hor**).[17] At 400 °C, a distinct sharp peak was observed at 918 cm^{-1}, which did not exist at 250 °C. Thus, the adsorption states in the flow of N_2 at 400 °C are completely different from those at 250 °C. In IR spectrum for N_2 adsorption observed at 400 °C in the wider wavenumber range (Figure S6), we can see obvious peaks at 3409, 1088, and 918 cm^{-1} and a broad peak with a peak around 1844 cm^{-1}. DFT calculations confirmed that the peak around 3409 cm^{-1} well matches 3404–3471 cm^{-1} for N–H bonds in NH species adsorbed on various sites of Ru(0001). Similarly, 3467 cm^{-1} was calculated for the antisymmetric vibration of N–H bonds in the NH_2 adsorbed on Ru (0001), and even the vibration of N–H bonds in NH_3 (3487 cm^{-1}) is comparable to the observed value of 3409 cm^{-1}. Calculated results for the vibrations of NH_x species on Ru(0001) are summarized in Figure S7. Here, we need to consider H sources for the NH formation. In this experiment, we treated catalysts with H_2 before all measurements and then confirmed the presence of OH groups formed on MgO during the pretreatment, which is the only possible H source in this experiment. Namely, at relatively lower temperatures such as 250 °C, OH groups are strongly immobilized on the Ru surface, whereas H atoms of OH groups are possibly dissociated and used for NH_3 formation at 400 °C. The peak observed at 1844 cm^{-1} corresponds to vibrations for **H-Ru** on the on-top site (1852 cm^{-1}) and for **N_2-Hor** on the bridge site (1851 cm^{-1}) of Ru_{153}, as reported previously.[17] To further assign the undefined 1088 and 918 cm^{-1} peaks, we focused on the delay of the adsorption intensity in phase, which was obtained by phase sensitive detection (PSD). PSD can notify the delay of response of the signal compared to the time for the introduction of a reaction gas (N_2 and H_2), as delay of the signal in phase ($\Psi_{PSD}(\theta)$, see SI) where $\Psi_{PSD}(\theta) = 0$ implies that signal intensity completely follows concentration of the reference gas. The $\Psi_{PSD}(\theta)$ value corresponds to the time taken to form the bond associated with its wavenumber. Regarding N_2 adsorption (Figure S8), we found IR peaks observed at 3409, 1844, 1088 and 918 cm^{-1} were characterized with $\Psi_{PSD}(\theta) = 53$, 85, 99, and 53°, respectively. If some peaks are identified with the same $\Psi_{PSD}(\theta)$, it strongly suggests that they are originated from identical adsorbed species. Thus, 918 cm^{-1} signal with $\Psi_{PSD}(\theta) = 53°$ can be correlated to 3409 cm^{-1} signal with $\Psi_{PSD}(\theta) = 53°$ and is accordingly assigned to the N–H stretching vibration. DFT calculation suggested that Ru–N vibration of adsorbed NH species located on the top site of Ru(0001) has a vibrational frequency of 822 cm^{-1} (Figure S7), which agrees with the experimental value of 918 cm^{-1}. The DFT calculations suggest that the experimental value of 918 cm^{-1} corresponds to the Ru–N vibration of NH adsorbed on the top site of Ru(0001), with a calculated vibrational frequency of 822 cm^{-1} (Figure S7). Although a slightly larger discrepancy exists between the calculated and observed wavenumbers for this specific vibrational mode compared to others, our comprehensive analyses of all possible adsorption sites in our model yield a reasonable conclusion. It is important, however, to acknowledge the challenge of fully matching the real experimental conditions and the idealized calculation model.

We hence distincted the 1088 cm^{-1} peak from N–H stretching vibration, whereas DFT calculation suggested that the peak is related to the wagging vibration of NH_3 on Ru(0001), which is characterized with 1126 cm^{-1} or Ru–N vibration involving an N atom binding to the top site on Ru(0001) with 1036 cm^{-1} (Figure S7). Thus, the formation of NH_x species and Ru–N bonds were confirmed at 400 °C although all observed peaks were not exactly assigned. Accordingly, we excluded **N_2-Ver** on the on-top and bridge sites, implying that N_2 molecules are dissociated on the Ru NP surface at 400 °C and AS can proceed via the reaction between dissociated N and H, namely ***dissociative*** mechanism.[4].

2.3. Co-adsorption of N_2 or H_2

Next, we observed the co-adsorption of N_2 and H_2 by introducing a mixed gas of N_2 and H_2. When the mixed gas was introduced after the H_2 pre-adsorption, a strong, sharp peak at 2085 cm^{-1} was solely observed at 250 °C (Fig. 2c top), whereas somewhat negative intensities were observed below 2000 cm^{-1}, suggesting that some adsorption sites for H species are used for N_2 adsorption. The 2085 cm^{-1} peak is assignable to **N_2-Ver** on the on-top Ru site,[17] similarly to 2071 cm^{-1} peak observed after introducing Ar (Fig. 2b top). We then exemplified the effect of the dissociated H atoms on the adsorption energy and N–N vibrational frequencies of **N_2-Ver** as shown in Figure S9, revealing that the N–N vibrational frequency increases when H atoms approach a vertically adsorbed N_2.[22] Thus, we can say that the blue shifted 2085 cm^{-1} peak for **N_2-Ver** on the on-top site under the mixed gas condition suggests certain interaction of the N_2 with an H atom that withdraws electrons from a Ru NP, which hinders the dissociation of the N–N bond. This result was already predicted by the previous DFT calculations for the Ru_{153} system.[22] Furthermore, the signal intensity for **N_2-Ver** at 2085 cm^{-1} decreased more quickly than that of the 2071 cm^{-1} peak observed after the Ar pre-adsorption (Fig. 2b top), which also suggests a weak interaction between N_2 and the H_2-treated surface. Co-adsorption after the H_2 pre-adsorption showed only very weak signals around 2000 cm^{-1} at 400 °C (Fig. 2c), which suggests that NH_3 formation hardly occurs even at relatively high temperatures on the surface that is once exposed to pure H_2. Thus, the Ru surface fully covered with H species cannot activate N_2 molecules for the progress of AS reaction even at 400 °C.

In contrast, various absorption peaks were observed when a mixed gas was introduced after the pre-adsorption with N_2 at both temperatures. DFT calculations suggested that a strong peak observed around 1917 cm^{-1} at 250 °C (Fig. 2d top) is assignable to **H-Ru** on the top of a Ru vertex atom (1921 cm^{-1}), which is located in close proximity to another H atom. The H–H distance corresponding to this frequency was calculated to be 2.114 Å, as shown in Figure S10. In addition, we found weak peaks around 1620 and 1176 cm^{-1} at 250 °C (Fig. 2d top), which accord with wavenumbers predicted in the previous DFT studies; 1642–1659 cm^{-1} for some configurations of **N_2-Hor** on bridge sites of Ru_{153} and 1162–1183 cm^{-1} for a few N_2 molecules interacting on the 4F sites of Ru_{153}.[17] Similarly, 1164–1187 cm^{-1} for the **H-Ru** formed on the 3F sites of Ru_{153} is also another possible mode.[22] Meanwhile, DFT calculations conducted in this study for NH_3 adsorbed on the top site of Ru(0001) showed that scissoring (1581 cm^{-1}) vibrational modes of NH_3 are in good agreement with the observed peaks at 1620 cm^{-1} (Fig. 2d top). Similarly, we found that the 1176 cm^{-1} peak is related to rocking vibrations of N_2H horizontally adsorbed on the Ru_{153} surface (**N_2H-Hor**), of which vibrational wavenumbers were calculated to be in the range from 1112 to 1195 cm^{-1}. The detailed DFT results are summarized in Fig. S11a. Thus, AS reactions are developed via the formation of horizontally adsorbed N_2H at 250 °C as shown in Fig. 3a, which is denoted as ***horizontally associative*** mechanism.

It should be noted that a sharp negative peak and broad negative intensities were observed at 2148 cm^{-1} and below 1000 cm^{-1} at 250 °C in the flow of the mixed gas after the N_2 pre-adsorption (Fig. 2d top). Based on a previous report, we have correlated the 2148 cm^{-1} peak to **N_2-Ver** on a facet of Ru NPs, namely, wavenumbers were calculated to be in the range from 2163 to 2192 cm^{-1},[17] which is larger than those for **N_2-Ver** on a vertex. It should be noted that we did not observe **N_2-Ver** on a facet after H_2 pre-adsorption (Fig. 2c top). This is because all absorption sites on facets are already occupied by H species during H_2 pre-adsorption. The negative regions below 1000 cm^{-1} correspond to vibrations for **N_2-Hor** at 3F or 4F sites,[17] where N_2 molecules are highly activated. Thus, it is acceptable that vertically adsorbed N_2 molecules on a facet are transferred to horizontally adsorbed ones and then converted to NH species. Interestingly, the negative absorbance at 2148 cm^{-1} became positive just after switching to pure N_2 (Fig. 2d top), then decreased to zero at 156 s whereas the constantly positive signals were observed below 1100 cm^{-1}. Thus, we found the Ru sites on the facet becomes vacant during NH_3 formation in the presence of both N_2 and H_2 and can act as recoverable adsorption sites for N_2, which drives

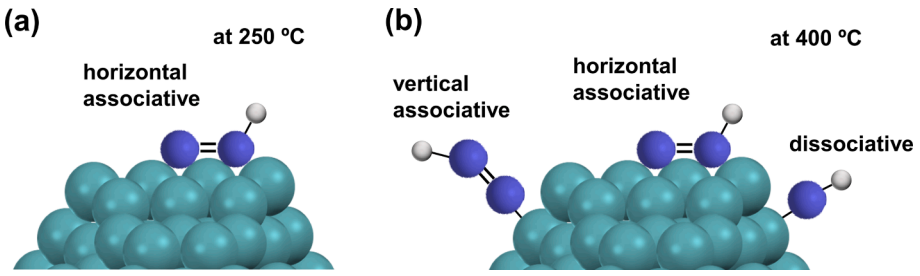

Fig. 3. Possible intermediate species in AS reactions at (a) 250 °C and (b) 400 °C.

the continuous AS reaction.

At 400 °C, we could see a peak around 1277 cm^{-1}, which can be assigned to the N–N bond vibration (1284 cm^{-1}) of **N_2H-Hor** at a bridge site between a vertex and edge atoms of Ru_{153} (Figure S11a). However, a broad peak having a maximum of around 1797 and 1662 cm^{-1} did not match the results from the DFT calculations for H, H_2, NH_3, NH_2, and NH species on Ru. Instead, DFT calculations could assign both two peaks to the N–N bond vibration of the vertically adsorbed N_2H (**N_2H-Ver**) on a vertex atom of Ru_{153} (Figure S11b). Depending on the position of remaining dissociated H atoms, the N–N vibrational frequency can become more red-shifted to 1688 cm^{-1}, which is in good agreement with the experimental peak at 1662 cm^{-1}. These results suggest that AS reactions proceed not only via ***horizontally associative*** mechanism but also via the formation of vertically adsorbed N_2H species, namely, ***vertically associative*** mechanism, at 400 °C (Fig. 3b).

As we already mentioned, we could not observe vibration for **N_2-Ver** at 400 °C after the Ar and N_2 pre-adsorption (Fig. 2b and 2d bottom), suggesting the lifetime of N_2 species related to **N_2-Ver** is considerably short.

2.4. AS reaction process developed on Ru/MgO

Fig. 4a shows time-dependent change in absorbance of the 1176 cm^{-1} peak observed under the mixed gas conditions at 250 °C, which was assigned to **N_2H-Hor** on Ru (Fig. 2d, top). Remarkably, the absorbance reached the maximum at 13 s and became constant, implying that the system reached a steady state under the current reaction conditions. Then, we can draw a picture for the progress of AS reaction on Ru/MgO. In the presence of N_2 and H_2, continuous NH_3 formation is realized because 3 or 4 vacant sites are produced because three H and one N species are removed from the adsorption sites such as three Ru on-top sites for **H-Ru**, one for **N_2-Ver** and two for **N_2-Hor** during NH_3 formation (Fig. 4b). Thus, we assume that the progress of AS reactions is relevant to the transformation of vertically adsorbed N_2 from an on-top to a bridge site, which is composed of two Ru atoms. Fig. 5a describes the time-dependent change in the absorbance of peaks which were assigned to **N_2-Ver** on the on-top of a facet or edge, **N_2-Ver** on the bridge, **H-Ru**, and NH_3. Interestingly, the intensity for **N_2-Ver** on the bridge exhibited similar trend to those for **H-Ru** and NH_3, implying that **N_2-Ver** on the bridge is relevant to NH_3 formation, whereas the other two signals for **N_2-Ver** on the on-top sites showed different trends. To quantitatively evaluate the amount of N_2 intermediate species, Kubelka-Munk transform for the signal intensity was performed (inset of Fig. 5a), and the line-fitting in the range from 115 and 143 s was conducted. The results showed that the inclinations of the signal intensity for **N_2-Ver** on the on-top of Ru atom located on a facet (Δ_{top}) and the bridge ones (Δ_{bridge}) are -4.79×10^{-4} and 2.08×10^{-4} K-M unit/s, respectively, with a ratio of $\Delta_{top}/\Delta_{bridge} = -2.30$. This value matches the model where the elimination of two adsorption species on the on-top sites is needed for emergence of N species on one bridge site (Fig. 5b). In addition, our previous PSD analysis suggested that increase of signal intensity for **N_2-Ver** on the on-top site is considerably faster and slow transition of vertically adsorbed N_2 from an on-top to bridge site occurs.[17] Thus, we think that transformation of N_2 from on the on-top to bridge site is very important for the formation of horizontally adsorbed N_2, which is critical species for the progress of AS on Ru/MgO at 250 °C.

3. Conclusion

We have successfully observed adsorbed species changing with time on Ru/MgO under reaction conditions by in-situ DRIFTS-MES and DFT calculations, which elucidates not only the types of intermediates but also their adsorption states and sites on Ru/MgO. In particular, different thermal conditions were found to involve different reaction pathways of

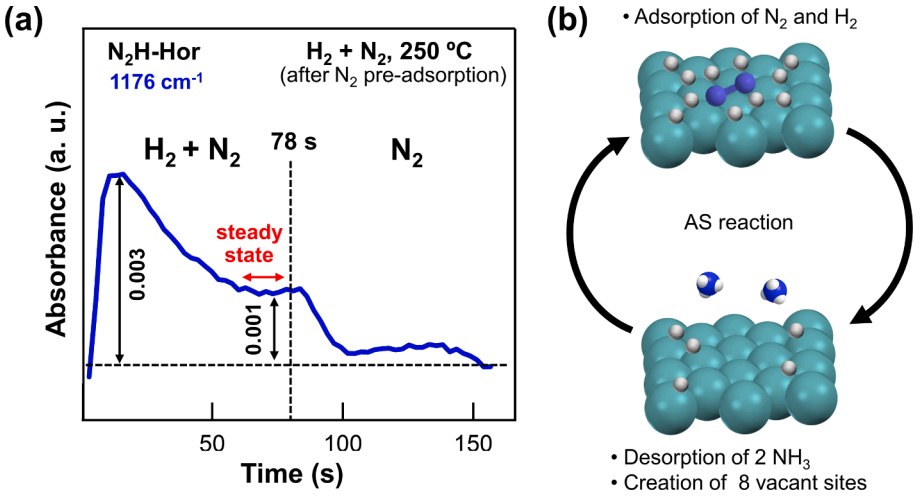

Fig. 4. (a) Time dependence of the absorbance for wagging NH_3 peak (1176 cm^{-1}) under the mixed gas condition at 250 °C after N_2 pre-adsorption. (b) Schematic image of the progress of AS reaction.

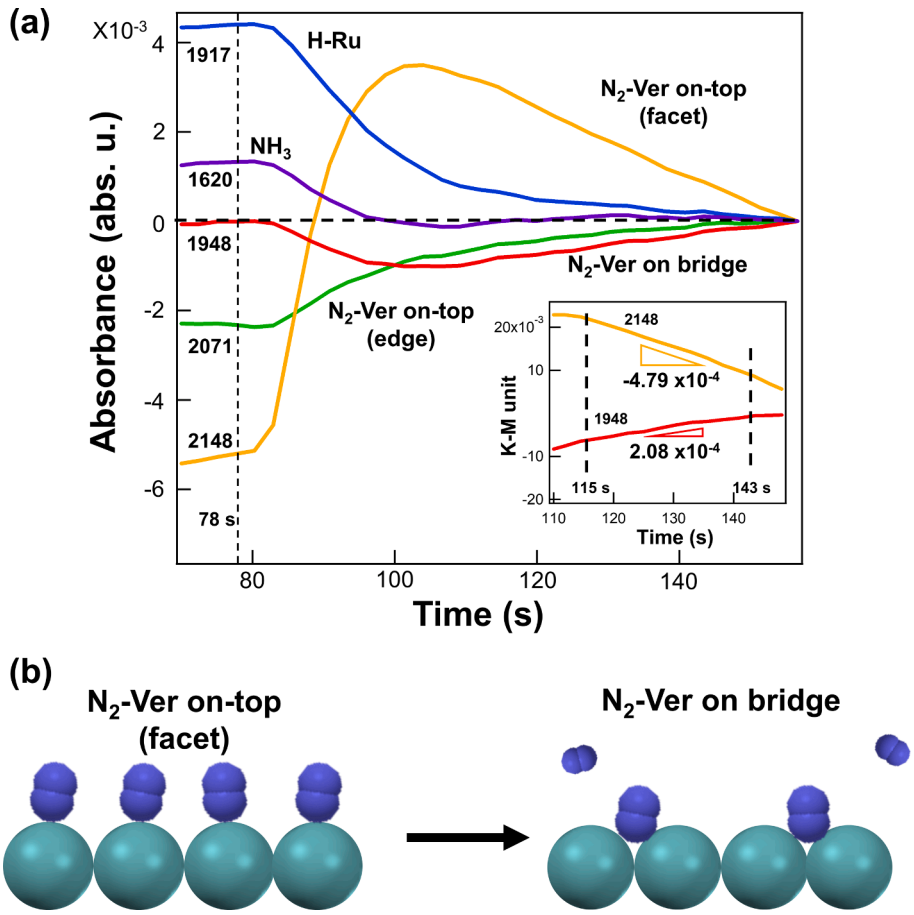

Fig. 5. (a) Time dependence of the absorbance for each adsorption state after the introduction of mixed gas at 250 °C (Fig. 2d top). Intensity of 2148 and 1948 cm^{-1} peaks in Kubelka-Munk unit, and their inclinations from 115 to 143 s are shown in inset. (b) Schematic image for transfer of vertically adsorbed N_2 from the on-top (facet) to bridge sites.

AS reaction on Ru NPs; only the ***horizontally associative*** mechanism runs at 250 °C, whereas three considerable mechanisms such as ***dissociative***, ***vertically*** and ***horizontally associative*** mechanisms are developed at 400 °C. Therefore, the catalyst design for accelerating ***horizontally associated*** mechanism is a key to promote AS reaction at lower temperatures. Furthermore, our PSD analysis revealed that the formation of vertically adsorbed N_2 on the bridge site is a hidden step to accelerate AS reaction. These exact descriptions about intermediate species dynamically changing on the catalyst surface would strongly support for rational design to create highly efficient catalysts.

4. Computational details

All calculations were based on the plane-wave DFT method implemented in the Vienna *ab initio* simulation package (VASP 5.6.2).[23] Perdew – Burke – Ernzerhof parametrization under the generalized gradient approximation was employed as the exchange–correlation functional together with the projector-augmented wave method.[24] Spin-polarized calculations were performed throughout the study with a plane-wave cutoff energy of 600 eV. The convergence criterion for all calculations was set as the point at which the difference in the total energy between the two ionic steps was less than 10^{-5} eV/atom (10^{-6} eV/atom for self-consistent-field iterations). The optimization of the hexagonal close-packed (hcp) bulk Ru was performed with 16 × 16 × 10 Monkhorst – Pack k-point mesh for the Brillouin zone integration, where all the atoms and the crystal volume were allowed to relax. After the optimization, the calculated lattice parameters, $a = 2.715$ and $c = 4.279$ Å, were in good agreement with the experimental values $a = 2.706$ and $c = 4.282$ Å.[25] Subsequently, the bulk was cleaved, and the Ru(0001) slab was constructed with seven atomic layers, from which the coordinates of the atoms in the bottom three layers of the slabs were kept frozen while the coordinates of the atoms in the four top layers were fully relaxed. The vacuum between the slabs was set to span a range of 17 Å to ensure no significant interaction between the slabs. The choice of Ru(0001) as the surface orientation is based on its exceptional stability among Ru surfaces. Previous studies have successfully employed a nanoparticle model consisting of two facets, {0001} and {10 $\bar{1}$ 1} to identify the adsorption states of H_2 and N_2. [17] Additionally, this model has helped in understanding the impact of H poisoning on Ru NPs.[22]. The optimization of the Ru(0001) was performed with 4 × 4 × 1 Monkhorst – Pack k-point mesh for the Brillouin zone integration. The interaction of the NH_x species was approximated by the adsorption energy, E_{ads}, calculated as:

$$E_{ads} = E_{Ru+adsorbate} - E_{Ru} - E_{adsorbate} \quad (1)$$

where $E_{Ru+adsorbate}$, E_{Ru}, and $E_{adsorbate}$ denote the total energies of NH_3, NH_2, NH, or N atoms interacting with the Ru(0001), the total energy of the pristine Ru(0001), and the total energies of isolated NH_3, NH_2, NH, and a N atom, respectively. According to this definition, negative adsorption energies denote more stable adsorbate–Ru interactions.

The optimization of the N_2H interacting with the hcp structure of the 1.58 nm diameter Ru nanoparticle, Ru_{153}, was performed at the Γ point in reciprocal space owing to the significant spatial extent of the system, where all the atoms were allowed to relax. Similarly for the interaction of N_2 on Ru_{153} pre-covered with two H atoms. The distance between neighboring image Ru nanoparticles was set as 15 Å to avoid interaction

between periodic images. The E_{ads} of N_2H on Ru_{153} was calculated as in equation (1), where $E_{Ru+adsorbate}$, E_{Ru}, and $E_{adsorbate}$ denote the total energies of N_2H interacting with the Ru_{153}, the total energy of the Ru_{153}, and the total energies of isolated N_2H, respectively. The structures of the N_2 together with the two H atoms binding to Ru_{153} are shown in Figure S11a.

The E_{ads} of N_2 on the H precovered Ru_{153} was calcualted as:

$$E_{ads} = E_{Ru+2H+N_2} - E_{Ru+2H} - E_{N_2}, \quad (2)$$

where $E_{Ru+2H+N_2}$, E_{Ru+2H}, and E_{N_2} denote the total energies of N_2 interacting with the Ru_{153} pre-covered with two H atoms, the total energy of the Ru_{153} with two H atoms, and the total energy of isolated N_2, respectively. The structures of the N_2 together with the two H atoms binding to Ru_{153} are shown in Figure S9.

The vibrational calculations were performed using central differences with atomic displacements of ± 0.015 Å in all three Cartesian directions. The dynamical matrix was constructed by displacing all the adsorbates' atoms that are interacting with the Ru nanoparticle and Ru (0001). For the NH_x species adsorbed on Ru(0001), the N-Ru atoms were also displaced. The self-consistent-field iterations convergence criterion was set to 10^{-8} eV/atom for all the vibrational calculations.

Declaration of Competing Interest

The authors declare that they have no known competing financial interests or personal relationships that could have appeared to influence the work reported in this paper.

Data availability

No data was used for the research described in the article.

Acknowledgements

We acknowledge funding from JSPS KAKENHI (JP18H05517, 22 K19088, JP19H05062, JP22H01758, 23H00313). The computations were performed using the computer resources offered under the category of General Projects by the Research Institute for Information Technology, Kyushu University.

Appendix A. Supplementary material

Supplementary data to this article can be found online at https://doi.org/10.1016/j.jcat.2023.07.020.

References

[1] R. Schlögl, Angew. Chem. Int. Ed. 42 (2003) 2004–2008.
[2] a) A. Valera-Medina, F. Amer-Hatem, A. K. Azad, I. C. Dedoussi, M. de Joannon, R. X. Fernandes, P. Glarborg, H. Hashemi, X. He, S. Mashruk, J. McGowan, C. Mounaim-Rouselle, A. Ortiz-Prado, A. Ortiz-Valera, I. Rossetti, B. Shu, M. Yehia, H. Xiao, M. Costa, *Energy Fuels* **2021**, *35*, 6964 – 7029; b) M. Aziz, A. T. Wijayanta, A. B. D. Nandiyanto, *Energies* **2020**, *13*, 3062; c) A. Yapicioglu, I. Dincer, *Renew. Sust. Energ. Rev.* **2019**, *103*, 96 – 108; d) N. Salmon, R. Bañares-Alcántara, *Sustain. Energy Fuels* **2021**, *5*, 2814 – 2839.
[3] S. Murata, K.I. Aika, J. Catal. 136 (1992) 110–117.
[4] K.I. Aika, Catal. Today 286 (2017) 14–20.
[5] C.J. Jacobsen, S. Dahl, B.S. Clausen, S. Bahn, A. Logadottir, J.K. Nørskov, J. Am. Chem. Soc. 123 (2001) 8404–8405.
[6] K.I. Aika, T. Takano, S. Murata, J. Catal. 136 (1992) 126–140.
[7] M. Hara, M. Kitano, H. Hosono, ACS Catal. 7 (2017) 2313–2324.
[8] K.I. Aika, H. Hori, A. Ozaki, J. Catal. 27 (1972) 424–431.
[9] K. Sato, S.I. Miyahara, Y. Ogura, K. Tsujimaru, Y. Wada, T. Toriyama, T. Yamamoto, S. Matsumura, K. Nagaoka, A.C.S. Sustain, Chem. Eng. 8 (2020) 2726–2734.
[10] S. Murata, K.I. Aika, J. Catal. 136 (1992) 118–125.
[11] M. Kitano, Y. Inoue, H. Ishikawa, K. Yamagata, T. Nakao, T. Tada, S. Matsuishi, T. Yokoyama, M. Hara, H. Hosono, Chem. Sci. 7 (2016) 4036–4043.
[12] K. Ooya, J. Li, K. Fukui, S. Iimura, T. Nakao, K. Ogasawara, M. Sasase, H. Abe, Y. Niwa, M. Kitano, H. Hosono, Adv. Energy Mater. 11 (2021) 2003723.
[13] K.K. Ghuman, K. Tozaki, M. Sadakiyo, S. Kitano, T. Oyabe, M. Yamauchi, Phys. Chem. Chem. Phys. 21 (2019) 5117–5122.
[14] a) H. Fang, D. Liu, Y. Luo, Y. Zhou, S. Liang, X. Wang, B. Lin, L. Jiang, *ACS Catal.* **2022**, *12*, 3938 – 3954; b) S. E. Siporin, R. J. Davis, *J. Catal.* **2004**, *225*, 359 – 368.
[15] a) B. Lin, B. Fang, Y. Wu, C. Li, J. Ni, X. Wang, J. Lin, C.-T. Au, L. Jiang, *ACS Catal.* **2021**, *11*, 1331 – 1339; b) L. Li, T. Zhang, J. Cai, H. Cai, J. Ni, B. Lin, J. Lin, X. Wang, L. Zheng, C.-T. Au, L. Jiang, *J. catal.* **2020**, *389*, 218 – 228; c) Y. Zhou, X. Peng, T. Zhang, H. Cai, B. Lin, L. Zheng, X. Wang, L. Jiang, *ACS Catal.* **2022**, *12*, 7633 – 7642.
[16] a) Y. Zhang, X. Peng, J. Deng, F. Sun, J. Cai, Y. Zhou, J. Ni, B. Lin, L. Zheng, X. Wang, J. Lin, L. Jiang, *J. Catal.* **2021**, *404*, 440 – 450; b) M. Y. Aslan, E. Mete, D. Uner, *Faraday Discuss.* **2023**.
[17] D.S.R. Rocabado, T.G. Noguchi, S. Hayashi, N. Maeda, M. Yamauchi, T. Ishimoto, ACS nano 15 (2021) 20079–20086.
[18] a) J.-M. Andanson, A. Baiker, *Chem. Soc. Rev.* **2010**, *39*, 4571 – 4584; b) F. Meemken, P. Müller, K. Hungerbühler, A. Baiker, *Rev. Sci. Instrum.* **2014**, *85*, 084101; c) P. Müller, I. Hermans, *Ind. Eng. Chem. Res.* **2017**, *56*, 1123 – 1136.
[19] a) D. Baurecht, U. P. Fringeli, *Rev. Sci. Instrum.* **2001**, *72*, 3782 – 3792; b) A. Urakawa, T. Bürgi, A. Baiker, *Chem. Eng. Sci.* **2008**, *63*, 4902 – 4909; c) D. Baurecht, I. Porth, U. P. Fringeli, *Vib. Spectrosc.* **2002**, *30*, 85 – 92.
[20] F. Rosowski, A. Hornung, O. Hinrichsen, D. Herein, M. Muhler, G. Ertl, Appl. Catal. A-Gen. 151 (1997) 443–460.
[21] H. Iriawan, S.Z. Andersen, X. Zhang, B.M. Comer, J. Barrio, P. Chen, A.J. Medford, I.E.L. Stephens, I. Chorkendorff, Y. Shao-Horn, Nat. Rev. Methods Primers 1 (2021) 56.
[22] D.S.R. Rocabado, M. Aizawa, T.G. Noguchi, M. Yamauchi, T. Ishimoto, Catalysts 12 (2022) 331.
[23] a) G. Kresse, J. Hafner, *Phys. Rev. B* **1993**, *47*, 558; b) G. Kresse, J. Furthmüller, *Phys. Rev. B—Condens. Matter Mater. Phys.* **1996**, *54*, 11169–11186; c) G. Kresse, J. Furthmüller, *Comput. Mater. Sci.* **1996**, *6*, 15–50.
[24] P.E. Blöchl, Phys. Rev. B 50 (1994) 17953–17979.
[25] J.W. Arblaster, Platinum Metals Rev. 57 (2013) 127–136.